THE AMERICAN SOCIETY OF MECHANICAL ENGINEERS
345 E. 47th St., New York, N.Y. 10017

96-GT-42

DETAILED VELOCITY AND TURBULENCE MEASUREMENTS OF THE PROFILE BOUNDARY LAYER IN A LARGE SCALE TURBINE CASCADE

Marina Ubaldi, Pietro Zunino, Ugo Campora, Andrea Ghiglione
Istituto di Macchine e Sistemi Energetici
Università di Genova, Italy

ABSTRACT

Extensive measurements of velocity and turbulence have been performed by means of a two-component fibre-optic laser Doppler velocimeter, to investigate the profile boundary layer development on a large scale turbine cascade.

Flow field investigation has been integrated with data obtained by surface-mounted hot-film gauges in order to get direct information on the boundary layer nature and on its time varying characteristics.

Measurements were detailed enough to allow constructing mean velocity and Reynolds stress boundary layer profiles giving an in-depth description of the boundary layer development along both suction and pressure surfaces through laminar, transitional and turbulent regimes.

NOMENCLATURE

e hot film signal
e_0 hot-film signal at zero flow condition
f frequency
H_{12} shape factor = δ^* / θ
K acceleration parameter
$q\tau_w$ quasi wall shear stress
Re_θ momentum thickness Reynolds number = $U_e \theta / \nu$
s surface distance measured from leading edge
s_{max} surface length from leading to trailing edge
t time
Tu free-stream turbulence intensity, percent
u, v mean velocity components in streamwise and cross-stream directions
u', v' velocity fluctuations in streamwise and cross-stream directions
u_τ wall friction velocity = $\sqrt{\tau_w / \rho}$
u^+ dimensionless velocity = u / u_τ
U_e local free-stream velocity
w surface velocity
w_1 upstream velocity
y normal distance from the wall
y^+ dimensionless distance from the wall = $y u_\tau / \nu$
δ^* bouodary layer displacement thickness
θ boundary layer momentum thickness
ν kinematic viscosity
ρ fluid density
τ_w wall shear stress

Subscripts

1 cascade inlet
2 cascade outlet

Overbar

— time averaged

1. INTRODUCTION

Wakes from turbine blades are unsteady in character, because of the formation of large organised vortical structures, known as von Karman vortex street. This phenomenon is well known in cylinders, especially at moderate Reynolds numbers, but there is still lack of quantitative information in the turbine field (Cicatelli and Sieverding, 1995). Vortex shedding is a cause of energy losses, periodic mechanical loading, vibrations and noise. Furthermore, difficulties have been found to predict correctly the wake flow characteristics, even with advanced Navier Stokes codes, mainly because of turbulence models inappropriate to handle highly anisotropic unsteady flows.

At present experimental and theoretical aspects of the problem are being investigated in the framework of a BRITE Euram project by several European research institutes. The experimental activity is carried out with different complementary techniques on flat plates

Presented at the International Gas Turbine and Aeroengine Congress & Exhibition
Birmingham, UK — June 10-13, 1996

and large scale cascades of a turbine profile designed at VKI. Results of this research will be published in future.

Frequency and energy associated with vortex shedding are highly dependent on the boundary layer state at the blade trailing edge (Sieverding and Heinemann, 1989). For this reason wake flow studies cannot leave out of consideration an accurate investigation of the boundary layer development on both suction and pressure sides of the profile which generates the wake. The present paper reports the results of the experimental effort to document in detail the profile boundary layer development in the BRITE large scale cascade, including its turbulence characteristics.

Due to inherent measurement difficulties in the exceedingly thin blade boundary layers, complete velocity profiles (e.g. Hoheisel et al., 1987, Mee et al., 1990) and turbulence distributions (e. g. Hodson, 1983) are less frequent for turbine cascades than for compressor cascades (e. g. Deutsch and Zierke, 1988, Dong and Cumpsty, 1990, Elazar and Shreeve, 1990, Schulz et al., 1990, Wunderwald and Fottner, 1995). Sharma et al. (1982) were able to obtain data detailed enough for representing complete velocity and streamwise turbulence profiles in the transitional and turbulent regimes of a boundary layer developing under free-stream velocity gradients representative of suction side turbine profiles. Their results offer a reference point for low speed, large Reynolds number boundary layer investigations in turbine cascades operating under steady flow conditions.

In the present investigation efforts were made to obtain a comprehensive description of boundary layer mean velocity and Reynolds stress development on both suction and pressure sides, including laminar and transition regions. Most of the investigation was carried out by means of a four-beam fibre-optic laser Doppler velocimeter with burst spectrum processors. Direct information on the boundary layer condition was provided by analysing the fluctuating signals from surface-mounted hot-film gauges.

2. EXPERIMENTAL DETAILS

2.1 Test Facility

The experiments were carried out in the low speed wind tunnel of IMSE (Istituto di Macchine e Sistemi Energetici), which consists of a blow down continuous operating circuit with an open test section. A centrifugal blower driven by a 70 kW a.c. motor equipped with an electronic frequency converter supplies a flow rate of 9 m^3/s at the pressure of 4000 Pa, when the rotational speed is 1500 rpm. A contraction with area ratio 8.63 and mesh screens of appropriate characteristics provide a low turbulence uniform flow in the 500x300 mm test section ($Tu \cong 1$ percent based on the streamwise fluctuations).

The main instrumentation of the wind tunnel consists of miniature pressure probes, wall pressure tappings, scanivalve and resistive pressure transducers, a four channel constant temperature anemometer, a 2D fibre-optic laser Doppler velocimeter, a multi-channel PC based fast sampling data acquisition system with large storage capability. The test section is equipped with an automated three-axis probe traversing mechanism controlled by the data acquisition computer.

The blade boundary layer development was surveyed on the suction and pressure sides of the central blade of a three-blade large scale turbine linear cascade. The blade profile, designed at VKI, is representative of a high efficiency gas turbine nozzle blade.

The blade trailing edge is enlarged ($t/c = 0.05$) for lowering the vortex shedding frequency and contemporaneously increasing the strength and the scale of the phenomenon. For the same reasons a three blade configuration has been selected allowing larger blade dimensions, which are also favourable for the present boundary layer investigation. The blade chord is 300 mm, the pitch to chord ratio g/c is 0.7 and the aspect ratio h/c is 1.

The three blades made of epoxy resin are cantilevered from an horizontal aluminium plate with the span aligned with the vertical direction. A large Plexiglas levelled plane constitutes one of the carriages of the probe traversing mechanism and forms part of the cascade upper endwall. The spanwise gap between blade tips and the movable endwall is set at 0.4 mm.

The central blade is instrumented at midspan with 54 pressure tappings of 0.8 mm diameter. The two lateral blades are partially instrumented, on the suction side and on the pressure one respectively, for a total of 56 pressure tappings. When LDV and surface-mounted hot-film investigations had to be performed, the instrumented central blade was replaced with a mat black painted one.

During the experiment the cascade was operating at an isentropic downstream Mach number $M_{2is} = 0.24$ and the Reynolds number based on the outlet flow conditions and chord length was $Re_{2is} = 1.6 \cdot 10^6$.

The cascade geometry is shown in Fig. 1 The main geometrical parameters of the cascade and the test conditions are summarised in Table 1. The coordinates of the blade are given by Cicatelli et al. (1994).

The secondary flow development in the cascade was moderate because of the continuous flow acceleration, the moderate flow turning ($\cong$ 70 deg) and the small inlet boundary layer displacement thickness. Two-dimensionality at midspan was verified by means of blade surface oil visualisations performed at VKI, and downstream spanwise probe traverses carried out at IMSE.

Due to the reduced number of blades, the establishment of periodic conditions represents a rather critical task. It was tried by modifying the curvature of two adjustable tailboards and by throttling two lateral apertures between the test section lateral walls and the lateral blades. The comparison of the midspan wall velocity distributions for the central blade and the lateral ones, shown in Fig. 2, indicates that very satisfactory periodicity conditions have been finally achieved.

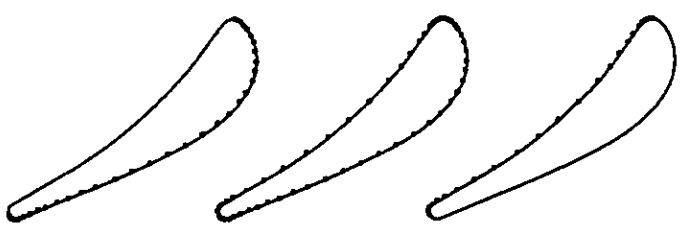

Fig. 1 Cascade geometry

2.2 Instrumentation and Experimental Procedure

LDV System and Measuring Procedure. To investigate the flow in the blade boundary layer, a four-beam two-colour fibre optic LDV system with back-scatter collection optics (Dantec Fiber Flow) has been used. The light source is a 300 mW argon ion laser operating at 488 nm (blue) and 514.5 nm (green).

The probe consists of an optical transducer head of 60 mm diameter connected to the emitting optics and to the photomultipliers by means of optic fibres. The front lens has a focal length of 400 mm. With a beam separation of 38 mm, the optical probe volume is 0.19 mm of diameter and 4 mm of length. The probe volume contains two sets of blue and green fringes (with approximate spacing of 5.1 μm and 5.4 μm respectively), which allow the contemporaneous measurement of the two velocity components in the plane perpendicular to the optical axis of the probe. A Bragg cell is used to apply a frequency shift (40 MHz) to one of each pair of beams, allowing to solve directional ambiguity and to reduce angle bias.

The optical access to the cascade flow has been made possible through a 300x200 mm large, 3 mm thick removable borosilicate glass window inserted in the X-axis carriage (top wall of the cascade). The probe volume was oriented with the larger dimension along the spanwise direction in order to have better spatial resolution in the wall normal direction. In order to measure contemporaneously streamwise and normal velocities close to the blade surface, the optical axis was slightly tilted (about half the angle of the intersecting beams).

The probe was traversed using a three-axis computer controlled probe traversing system. The motion was transmitted to the carriages by stepping motors through preloaded ball-screw assembly, with a minimum linear translation step of 8 μm. The origin for the velocity profile was estimated by visual inspection of the intersection of the laser beams approaching the blade surface and by survey of the analog signal of the photomultiplier on a digital oscilloscope. Repeatability in establishing the origin was estimated to be ± 0.03 mm.

The flow was seeded with a 0.5-2 μm atomised spray of mineral oil injected in the flow at about 2 chord upstream of the cascade leading edge.

Table 1 Cascade geometry and test conditions

Cascade Geometry			
Chord length	c	= 300	mm
Pitch to chord ratio	g/c	= 0.7	
Aspect ratio	h/c	= 1.0	
Inlet blade angle	β'_1	= 0	deg
Gauging angle	$\beta'_2 = \sin^{-1}(o/g)$	= 19.1	deg
Number of blades	N	= 3	
Test Conditions			
Relative inlet total pressure	p_{t1}	= 3060	Pa
Inlet total temperature	T_{t1}	= 293	K
Inlet turbulence intensity	Tu	= 1	%
Inlet flow angle	β_1	= 0	deg
Outlet isentropic Mach number	M_{2is}	= 0.24	
Outlet isentropic Reynolds number	Re_{2is}	= $1.6 \cdot 10^6$	

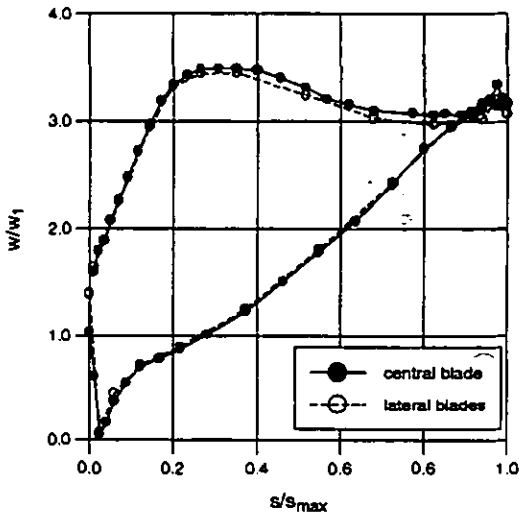

Fig. 2 Surface velocity distribution

The signals from the photomultipliers were processed by two Burst Spectrum Analysers (Dantec BSA). The measurements of the two velocity components were made in coincidence mode. A typical value of the data rate was 2000 Hz in the outer part of the boundary layer, falling off to about 100 Hz in the inner part. For each measuring point 30000 samples were collected to obtain statistically accurate averages.

Pressure and suction side boundary layers have been surveyed by means of 35 traverses normal to the blade surface at midspan. The location of the boundary layer traverses and their corresponding reference numbers are shown in Fig. 3. Each boundary layer traverse is constituted by 29 measuring points. The distance between adjacent points was set at 0.05 mm in the region of the boundary layer close to the wall and was progressively increased in the outer part. The first point was set at a distance of 0.05 mm from the estimated wall position. At this position 25 percent of the probe volume was imbedded in the wall and strong background reflections were observed in the photomultiplier output on the oscilloscope. Nevertheless data were processed with a validation of the order of 10 percent after an appropriate selection of the processor bandwidth.

LDV Error Estimate. A comprehensive review of errors in laser-Doppler velocimetry measurements and guidelines to evaluate them are given by Boutier (1991) and, in the case of turbomachinery applications, by Strazisar (1986). A specific evaluation of errors for frequency domain processors is given by Modarress et al. (1988).

The error on the instantaneous velocity due to random noise from the photomultiplier tube depends on the background scattered light and on the processing technique. BSA can measure with a signal to noise ratio as low as -10 dB, without apparent increase of the standard deviation (Modarress et al., 1988). The resolution of the BSA processor depends on the record length of the FFT and on the background noise, but also in the worst cases it was well below 1 percent of the mean velocity.

A statistical bias can occur because the arrival times of the measurable particles are not statistically independent on the flow velocity which brings them in the probe volume. If the velocity is not constant in time, the resulting non uniform data sampling causes an error when simple arithmetic averages are performed. The magnitude of the bias is of the order of the square of the turbulence intensity based on the local mean velocity. To determine correct mean and turbulence quantities, residence-time weighted averages (Buchhave et al., 1979) have been applied.

Angle bias occurs when the particle trajectories are not normal to fringe orientation. Moving the fringe pattern in the probe volume by means of the Bragg cell minimises this error.

Errors due to velocity gradient can affect both mean and rms velocities. In the region near to the wall, the false turbulence due to the finite dimension of the probe volume can constitute a significant part of the measured streamwise velocity variance. Karpuk and Tiederman (1976) showed that, in case of linear mean velocity variation, the weighted-average of individual realisations is an unbiased estimate of the time-averaged velocity at the centre of the probe volume. Furthermore, they proposed a correction for the rms velocities, assuming a linear variation of the mean velocity across the probe volume. According to that analysis the root mean square of the streamwise velocity fluctuations has been corrected to obtain an unbiased estimate of the turbulence at the centre of the probe volume. Comparison between laser Doppler and hot-wire turbulence measurements provided confidence in the correction. In the free-stream region the comparison showed also that the laser Doppler turbulence intensity results were systematically higher of 0.3 percent. This false turbulence was probably due to an imprecise location of the beam waists in the probe volume producing fringe distortion. The false turbulence becomes irrelevant within the boundary layer, where the true turbulence increases.

Finally the statistical uncertainty in mean velocity and standard deviation is kept low because of the large number of data sampled for each measuring point (30000). Uncertainties of 0.1 percent and 0.8 percent have been evaluated for the mean and the rms velocities in case of 10 percent turbulence intensity and with a confidence level of 95 percent. In the near wall region, where the turbulence intensity evaluated using the local mean velocity instead of the free-stream velocity can increase of an order of magnitude, the large number of sampled data is sufficient to maintain the uncertainty of the mean velocity lower than 1 percent.

Surface Hot-Film Measurements. To help interpreting the boundary layer nature as well as to gain information on its unsteady characteristics, surface-mounted hot-film gauge measurements were performed in addition to LDV investigations.

A single-sensor hot-film element (Dantec 55R47) was employed. The sensor consists of a 0.1x0.9 mm thin nickel film applied by vapour deposition on a 50 μm thick polyimide substrate. The gauge was glued on a 25 μm thick strip of acetate of length appropriate to avoid any surface discontinuity near the sensor. The strip was fixed on the blade surface by means of a thin bi-adhesive tape and easily repositioned to investigate the whole blade surface. In this way the local discontinuity is limited to a 50 μm step, while the blade shape modification can be considered negligible, as the total thickness of

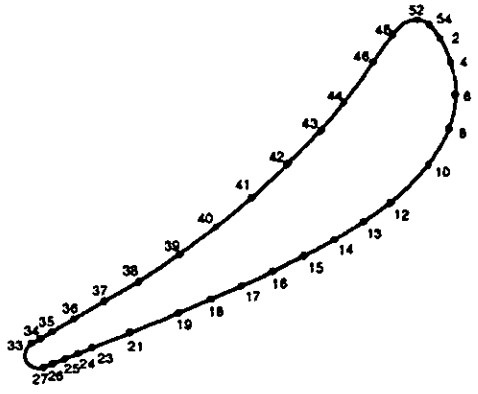

Fig. 3 Boundary layer measuring stations

the added layer is less than 0.2 mm and the nominal blade chord is 300 mm. Measurements were performed in all the boundary layer traversing points shown in Fig. 3 and in some intermediate points.

The film element was connected to a constant-temperature hot-wire unit (Dantec 55M10, 55M17), which maintains the film at the selected temperature difference (60 °C) with respect to the fluid. The system frequency response, deduced by a square wave test performed with the probe exposed to the flow, was found to exceed 20 kHz. An antialiasing low-pass filter with a cut-off frequency of 20 kHz was applied to the anemometer signal before it was sampled at a frequency of 50 kHz by means of a 12 bit A/D converter board.

Due to analogy between heat and momentum transfer in boundary layers, the local instantaneous wall shear stress is related to the rate of heat transfer from the hot sensor to the fluid (Bellhouse and Schultz, 1966)

$$\tau_w = k\left[\left(e^2 - A^2\right)/\Delta T\right]^3 \qquad (1)$$

where e is the instantaneous voltage and ΔT is the temperature difference between sensor and fluid. The calibration of this type of probe is rather critical and very seldom tried but, as was pointed out by several authors (e. g. Oldfield et al., 1981, Hodson, 1985, Pucher and Göhl, 1987, Hourmouziadis et al., 1987, Halstead et al., 1995), useful information on the boundary layer transition and separation phenomena, as well as on its unsteady properties, can be obtained by a semi-quantitative analysis. As pointed out by Hodson (1985), the rate of heat transferred to the substrate is proportional to the square of the constant A, and can be approximated by the square of the zero flow voltage e_0^2. Furthermore, if the temperature of the blade is equal to the air temperature, the temperature difference ΔT is proportional to e_0^2 and eq. (1) can therefore be written as

$$\tau_w \equiv k\left[\left(e^2 - e_0^2\right)/e_0^2\right]^3 \qquad (2)$$

The quantity $\left[\left(e^2 - e_0^2\right)/e_0^2\right]^3$ can be referred as instantaneous quasi wall shear stress $q\tau_w$. The analysis of the hot-film data was performed following the indications of Schröder (1991) and Halstead et al. (1995). The signals were analysed both in time and in frequency domain. For each measuring position, a total of 172032 data was taken. Time averages, root mean squares and third order moments of the instantaneous quasi wall shear stress were evaluated for each point and plotted in function of the streamwise coordinate along

pressure and suction sides. At each position a power spectral distribution of the instantaneous data was obtained by operating over averages of 20 FFT's, performed on partially overlapping blocks of 16384 values.

3. RESULTS AND DISCUSSION

3.1 Surface Velocity Distributions

The surface velocity distributions for both central and lateral blades are shown in Fig. 2. The abscissa s/s_{max} is the fraction of surface length from leading to trailing edge. The distributions are of the front-loaded type with a moderate suction side diffusion rate: a velocity maximum $w_{max}/w_2 = 1.13$ is located at $s/s_{max} = 0.30$. The moderate deceleration following the overshoot does not appear to cause any evident boundary layer separation. On the pressure side the flow accelerates continuously.

The influence of the streamwise velocity gradient on the boundary layer developmment can be described in terms of the acceleration parameter $K = \frac{\nu}{U_e^2}\frac{dU_e}{ds}$.

The onset of transition depends on boundary layer local development, free-stream turbulence level and flow acceleration. The momentum thickness Reynolds number at transition onset $Re_{\theta t}$ increases with the increase of the acceleration parameter and the decrease of the free-stream turbulence (Mayle, 1991). In case of large turbulence intensity, $Re_{\theta t}$ appears to be correlated only with the free-stream turbulence and the transition criteria for zero pressure gradient flow can be used (Hourmouziadis, 1989: $Re_{\theta t} = 460\,Tu^{-0.65}$; Mayle, 1991: $Re_{\theta t} = 400\,Tu^{-5/8}$).

Making use of the above mentioned correlation for $Re_{\theta t}$ and the laminar separation criterion of Thwaites (1949) $Re_\theta^2 K = -0.082$, Mayle (1991) defines a critical acceleration parameter for transition and separation, which is a function of the turbulence level: $K_{crit} = -5.13\cdot10^{-7}\,Tu^{5/4}$. For $K > K_{crit}$ transition occurs before laminar boundary layer separation, while for $K < K_{crit}$ separation precedes transition.

The distributions of the acceleration parameter K for both pressure and suction sides are represented in Fig. 4. On the pressure side the parameter remains positive from leading to trailing edge. On the suction side, on the contrary, it changes sign at $s/s_{max} = 0.30$ and remains negative until 0.80.

In the same figure the lines $K = K_{crit}$ and $K = 3\cdot10^{-6}$ are depicted. This latter represents a limiting value for reverse transition (Mayle, 1991). If K is greater than $3\cdot10^{-6}$ the forward transition cannot occur, hence the two lines delimit the region where natural or bypass transition can take place for the present experiment.

Due to the high chord Reynolds number, the negative values of K associated with the suction side flow deceleration remain moderate and higher than K_{crit}, avoiding that laminar separation precedes transition, even with a relatively low free-stream turbulence level.

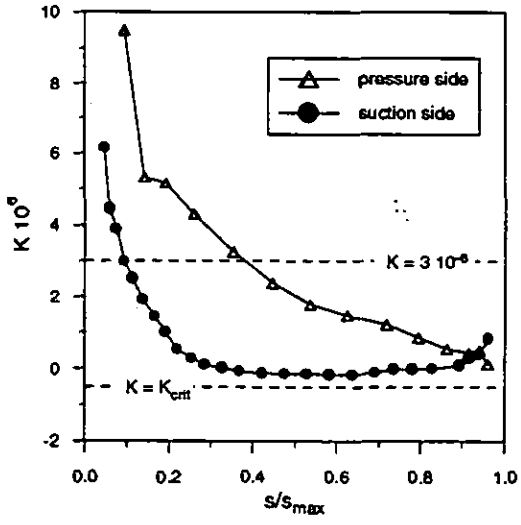

Fig. 4 Distribution of the acceleration parameter

As shown later in section 3.3, in the present investigation, with a free-stream turbulence intensity nearly 1 percent, a value of about 300 has been found for $Re_{\theta t}$ on the suction side. On this side, the transition onset is located after the velocity maximum, in a region of moderate flow deceleration. On the pressure side, where the flow is continuously accelerating, it is more difficult to identify unambiguously the location for the transition onset.

3.2 Surface Hot Film Measurements

Measurements with flush-mounted hot-film gauges help identifying the locations of boundary layer transition onset and completion. Figures 5 and 6 show the distribution along the blade surfaces of the quasi wall shear stress $q\tau_w$, as defined by eq. (2), together with rms and skewness of the $q\tau_w$ fluctuations.

With reference to the suction side distributions (Fig. 5), characteristic positions associated with the transition process can be identified: the start of transition ST is located at the point where the rms values start to increase and skewness moves from zero to positive values. Approximately at this position $q\tau_w$ attains a relative minimum. The transition point (TP) is defined by the maximum of the rms distribution, which corresponds to a region of large positive gradient for $q\tau_w$ and to the position where the third-order moment (skewness) is passing through zero, decreasing from the positive region (laminar flow conditions occurring for a larger fraction of time), to the negative one (turbulent flow conditions more extended in time than laminar ones). Finally the end of transition (ET) can be identified by the rms return to a nearly constant value and by skewness return to zero.

Start of transition (ST), transition point (TP) and end of transition (ET) are located respectively at $s/s_{max} = 0.35$, $s/s_{max} = 0.48$ and $s/s_{max} = 0.60$, with a transition length of about 25 percent of the suction side surface length.

Local indications on the boundary layer state and on the transition time-dependent features can be deduced by the time traces of the hot-film gauge instantaneous outputs and the corresponding power

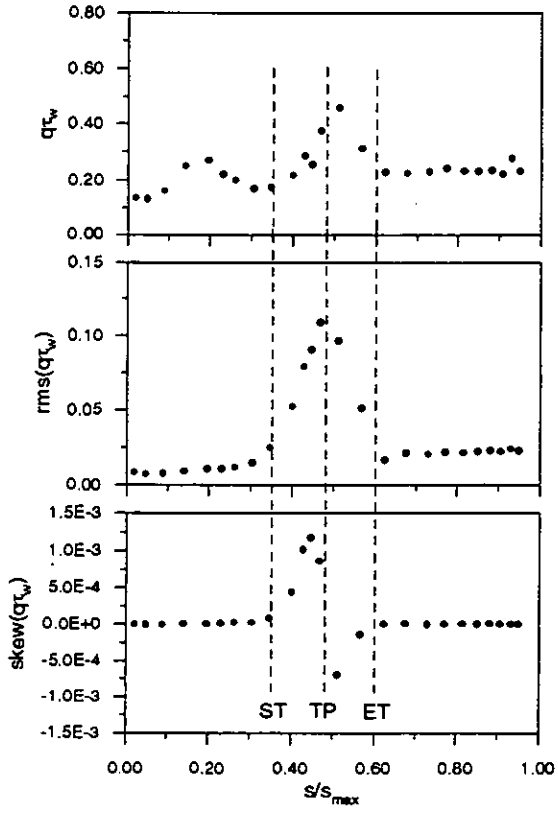

Fig. 5 Mean, rms and skewness distributions of the quasi wall shear stress on the blade suction side

density spectra. Results for the suction side boundary layer are shown in Fig. 7.

At station 8 ($s/s_{max} = 0.20$) the trace is typical of a laminar state with a low power density level ($1 \cdot 10^{-7}$) in the low frequency range. The peak in the power spectrum at about 45 Hz is believed to represent a selective response of the boundary layer to the natural random fluctuations in the free-stream (the initial hypothesis of instrument noise has been discarded, as this peak is not present at zero flow conditions and disappears in the boundary layer turbulent regions, even where the background power density in the low frequency range is of the order of 10^{-7}, as in the present distribution).

At the start of transition ST (station 12, $s/s_{max} = 0.35$), some turbulent bursts begin to appear, causing the power density level in the low frequency range to increase ($1 \cdot 10^{-6}$ for $f < 100$ Hz). At station 14 ($s/s_{max} = 0.46$), just before the transition point, the turbulent bursts become more frequent, causing the increase of the power density for the whole frequency range.

At station 15 ($s/s_{max} = 0.51$) the fraction of time during which the boundary layer is turbulent (higher instantaneous output voltage, high frequency fluctuations) is larger than the one during which the flow is laminar and the signal time trace exhibits a high output voltage level, interrupted by negative spikes representative of occasional laminar conditions. Compared with the previous position, the power density level is reduced in the low frequency range, but the

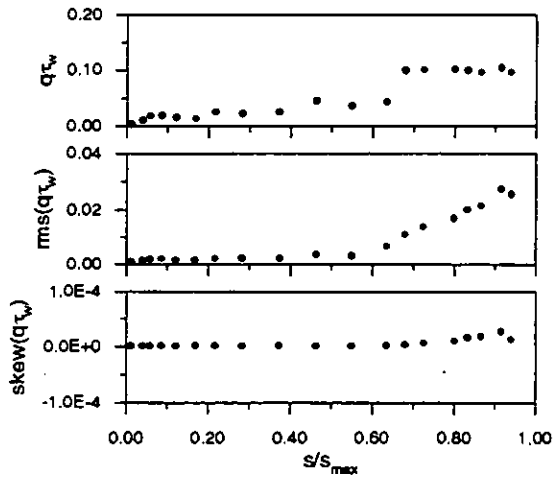

Fig. 6 Mean, rms and skewness distributions of the quasi wall shear stress on the blade pressure side

region of high power density is enlarged toward the higher frequencies, showing a typical distribution with plateau accompanied by the formation of a maximum (Schröder, 1991).

At point 18 ($s/s_{max} = 0.68$) the transition is completed and the time trace is typical of a turbulent boundary layer. The power density distribution, compared with those of the preceding points located in the transitional region, shows a lower level (in agreement with the rms distribution of Fig. 5), but extends more in the medium frequency range, decreasing with a moderate negative slope until 4 kHz. From this frequency the power density falls off with a negative slope of about -7.

On the pressure side the distributions of the mean value of $q\tau_w$ and of its second and third statistical moments (Fig. 6) indicate that the transition process is inhibited by the flow acceleration at least until $s/s_{max} = 0.6$ (in Fig. 4 the relaminarization limit was located at $s/s_{max} \cong 0.4$).

Compared with the suction side observations, here it is more difficult to identify a precise point for the transition onset, as the transition process is more gradual, due to the favourable velocity gradient. However rms and skewness start to move after $s/s_{max} = 0.6$, but at the trailing edge the transition process is not yet completed. The boundary layer remains in a laminar-transitional state all along the pressure side, as can be noted by observing the hot-film instantaneous traces of Fig. 8. This long transition process is typical of accelerating flows, as pointed out by Mayle (1991) and shown for instance by the investigation of Hodson (1985), Dong and Cumpsty (1990), and Keller and Wang (1994).

Due to the low free-stream velocity, heat convection is strongly reduced in the forward part of the pressure side and this causes a low level of the hot-film voltage output, which is progressively increasing from the leading edge to about 70 percent of the blade surface.

At station 46 ($s/s_{max} = 0.12$) the boundary layer appears to be in a laminar state with low power density in the high frequency range, oscillations in the low frequency range 10-200 Hz, and a peak at about 45 Hz similar to that observed in the laminar region on the suction side. The power density distributions are very similar until about $s/s_{max} = 0.6$. At station 39 ($s/s_{max} = 0.64$) the power density

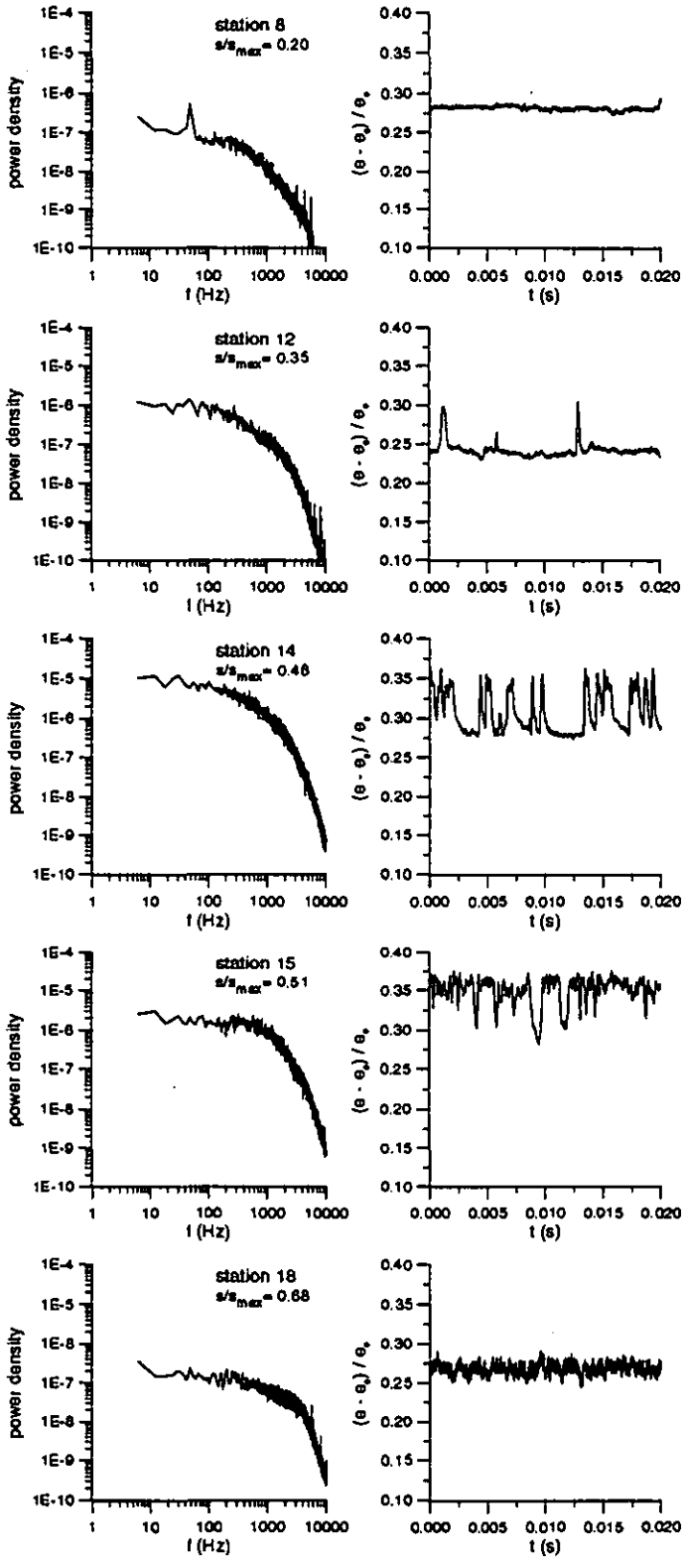

Fig. 7 Power density spectra and time traces of the hot-film signals on the blade suction side

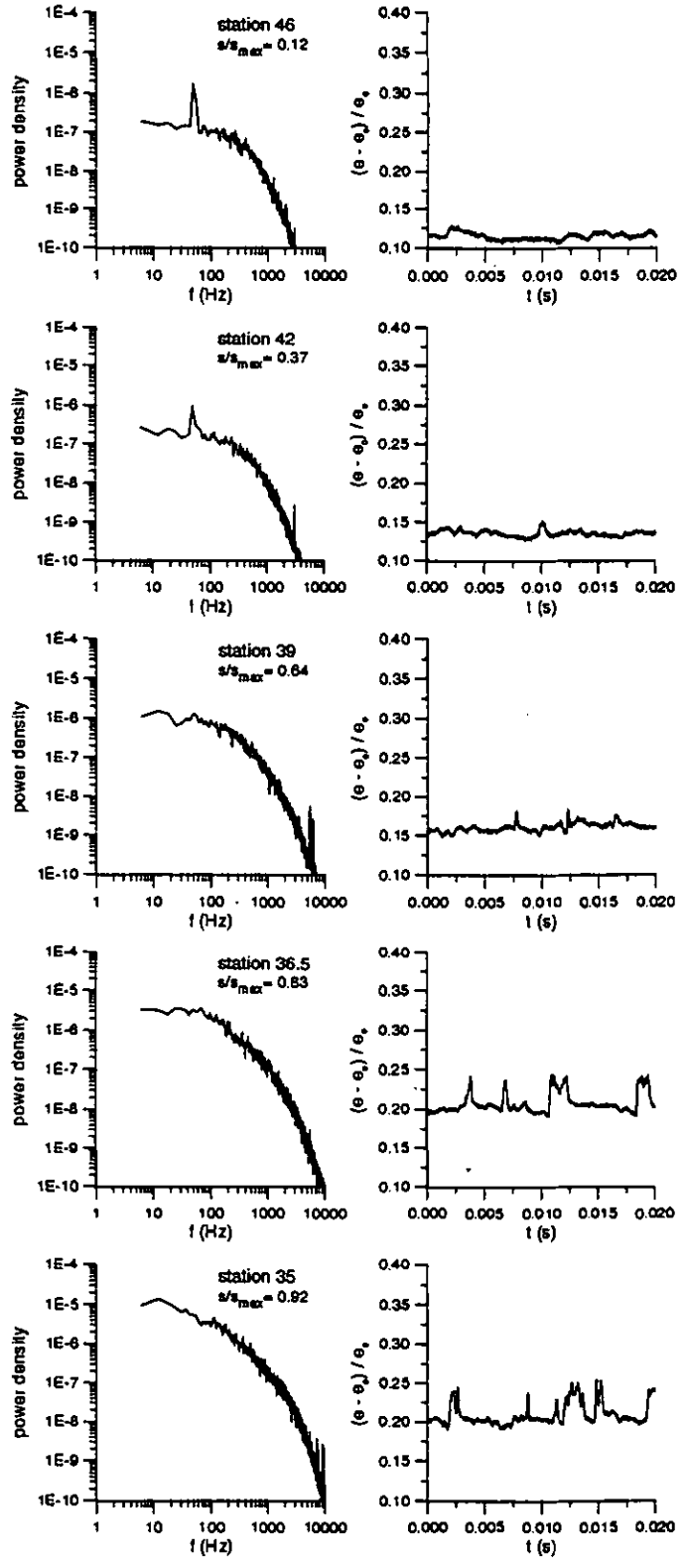

Fig. 8 Power density spectra and time traces of the hot-film signals on the blade pressure side

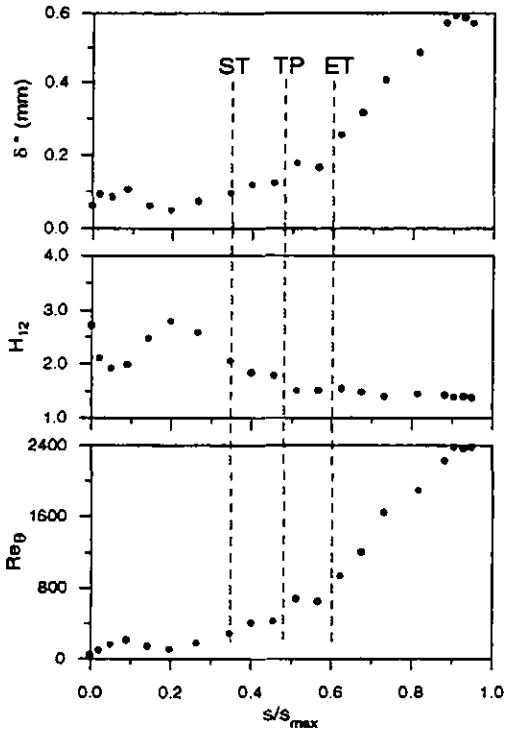

Fig. 9 Boundary layer integral parameters on the blade suction side

shows a slight increase in the whole frequency range, but the time trace looks still similar to the preceding ones. Only above $s/s_{max}=0.8$, at stations 36.5 ($s/s_{max}=0.83$) and 35 ($s/s_{max}=0.92$) the presence of turbulent bursts is evident.

3.3 Boundary Layer Integral Parameters

The boundary layer mean velocity profiles measured by means of LDV have been used to evaluate boundary layer integral parameters, such as displacement thickness δ^*, shape factor H_{12}, momentum thickness Reynolds number Re_θ and wall friction velocity u_τ. This latter has been determined by using Clauser chart in the turbulent regions, while, in laminar and transitional regions, it has been obtained by fitting the mean velocity data near the wall on the linear correlation $u^+=y^+$, as done by previous investigators (e. g. Sharma et al., 1982, Zhou and Wang, 1993). Distributions of the wall friction velocity have also been evaluated from the surface hot-film measurements, after having estimated the constant which relates $q\tau_w$ and τ_w to be the mean value obtained in the turbulent region of the rear suction side, where τ_w has been determined by using the Clauser chart. Agreement between the results obtained by means of the two different procedures (Fig. 11) is fairly good. In the transitional region on the suction side, due to the high free stream velocity, the value of y^+ for the measuring point nearest to the wall is larger than 10. Near wall mean velocity data, therefore, cannot longer be fitted on the linear correlation, as done for the transitional profiles on the pressure side, where y^+ values are lower. Hence the wall friction velocities in

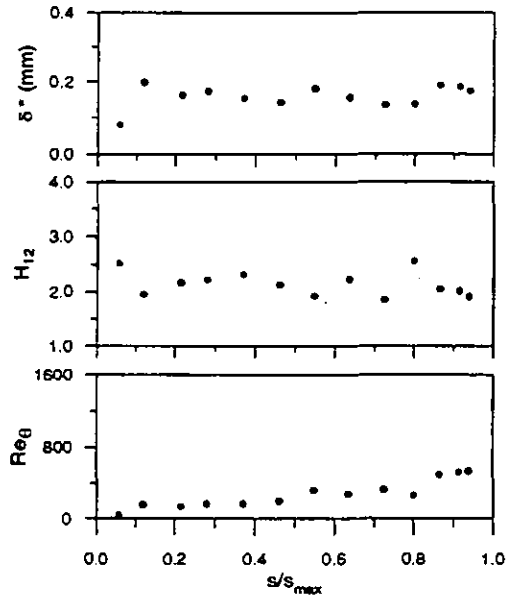

Fig. 10 Boundary layer integral parameters on the blade pressure side

the suction side transitional region are obtained only by means of the surface hot-film measurements.

The distributions of the integral parameters are given in Figs. 9 and 10, respectively for suction and pressure side. The distinctive points of the transition process ST, TP, ET, as deduced by the hot-film analysis, are marked on Fig. 9.

In the forward part of the suction side, the shape factor H_{12} decreases slightly below 2, while both δ^* and Re_θ increase, suggesting the hint of a transition phenomenon induced by free-stream fluctuations. The extremely thin boundary layer at this position however does not recommend excessive confidence in the calculated integral parameters. In this region the acceleration parameter K (Fig. 4) exceeds the relaminarization limit and a transition phenomenon should not occur.

The boundary layer remains laminar until $s/s_{max}=0.35$, position where the hot-film analysis has located the start of transition (ST). At this position the wall friction velocity has reached its minimum value, the shape factor H_{12} is about 2.0 and the momentum thickness Reynolds number is about 300. In presence of adverse pressure gradient, Re_θ increases rapidly to 400 at $s/s_{max}=0.40$. At the transition point (TP, $s/s_{max}=0.48$), H_{12} is about 1.8, while the wall friction velocity is near to its relative maximum.

The hot-film results indicate a transition length slightly larger than the one predicted by the distribution of the integral parameters. In fact at $s/s_{max}=0.52$ the boundary layer shape factor H_{12} is about 1.5, which is typical of a fully turbulent boundary layer, while the ET point from hot-film data is located at $s/s_{max}=0.6$.

On the pressure side, the integral parameter distributions of Fig. 10 confirm the laminar-transitional nature of the boundary layer from the leading to the trailing edge, due to the continuously accelerating flow. The displacement thickness δ^* remains always lower than 0.2 mm, H_{12} oscillates between 2.5 and 2.0. The lower free-stream

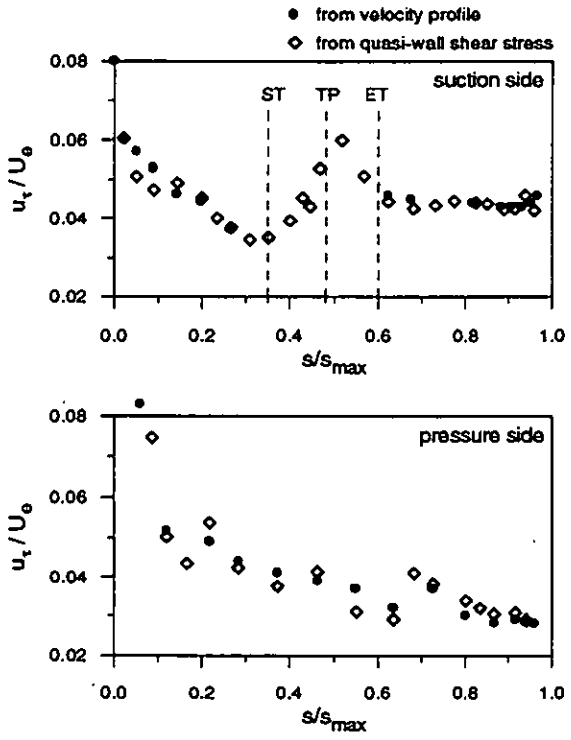

Fig. 11 Wall friction velocity distributions

velocity on the pressure side contributes to maintain the momentum thickness Reynolds number lower than 400 until $s/s_{max} = 0.8$. From this position toward the trailing edge, H_{12} decreases below the value of 2 and Re_θ overcomes the value of 400, indicating that transition is under way.

3.4 Velocity and Turbulence Profiles

The LDV instantaneous data have been weighted-averaged in order to obtain boundary layer profiles for the streamwise velocity u, streamwise and cross-stream rms components $\left(\overline{u'^2}\right)^{1/2}$, $\left(\overline{v'^2}\right)^{1/2}$ and Reynolds shear stress $-\overline{u'v'}$. Illustrative examples of velocity and turbulence profiles are given for the boundary layers developing along both suction (Figs. 12-15) and pressure sides (Figs. 16-17). First the profiles are represented in dimensional coordinates to provide an initial overview of the boundary layer development, then they are analysed in the inner layer variables.

Suction Side Boundary Layer. Figure 12 refers to boundary layer traverses performed in the laminar-transitional region of the suction side extending from the leading edge to $s/s_{max} = 0.46$.

Due to the external flow acceleration, from the leading edge to $s/s_{max} = 0.30$ the boundary layer remains extremely thin. In the laminar region the boundary layer thickness δ is nearly 0.2 mm, while in the transitional region (station 14, $s/s_{max} = 0.46$) δ has increased to about 0.7 mm.

The effect of transition on the mean velocity profiles appears as a velocity defect in the central part of the boundary layer. As regards the turbulence profiles, a general feature is represented by the strong anisotropy that characterizes transition. In the laminar region, both the components of the fluctuating velocity are low (the maximum of the streamwise component is about 2 m/s), but in the transitional region the streamwise fluctuating velocity shows a dramatic increase, with a maximum of about 13 m/s located at a distance from the wall of about 0.3 δ. As a consequence of the increase of the fluctuating velocities, also the Reynolds shear stress experiences an increase and a peak separated from the wall becomes evident (stations 12, 13, 14).

Actually the increase of the rms streamwise velocity during transition results by the combined effect of random turbulence and intermittent profile switching between laminar and turbulent states. To obtain true values of the turbulence quantities, such as Reynolds stress, conditional sampling of the laminar and turbulent phases should be considered, as made for instance by Kim et al. (1994). In the present investigation only time averages of the fluctuating velocities have been performed and the terms turbulence intensity and Reynolds stress refer to these quantities.

Figure 13 shows a set of velocity and turbulence profiles in the range $s/s_{max} = 0.57 - 0.95$, characterised by a turbulent development of the boundary layer. Station 16 ($s/s_{max} = 0.57$) is located just ahead of the transition end point identified by the hot-film investigation. At this position the boundary layer is not yet completely turbulent, as it can be deduced by comparing its mean velocity and turbulence profiles with those of the fully turbulent region. The streamwise fluctuating velocity still presents the peak separated from the wall typical of transitional states.

To examine in detail the experimental data in the region near the wall, the velocity profiles have been scaled in the inner layer variables ($u^+ = u/u_\tau$ and $y^+ = yu_\tau/\nu$) and are represented in semilogarithmic plots. The same abscissa y^+ is adopted for representing the streamwise and cross-stream turbulence intensities $\left(\overline{u'^2}\right)^{1/2}/U_e$, $\left(\overline{v'^2}\right)^{1/2}/U_e$ and the dimensionless Reynolds shear stress $-\overline{u'v'}/u_\tau^2$ (Figs. 14 and 15). The velocity profiles are compared with well established semi-empirical correlations for turbulent boundary layers (see for instance White, 1991):

- the linear correlation in the viscous sublayer range $y^+ \le 5$

$$u^+ = y^+ \tag{3}$$

- the law of the wall in the overlap layer range $35 \le y^+ \le 350$

$$u^+ = \frac{1}{k}\ln y^+ + B \tag{4}$$

with $k = 0.41$ and $B = 5$;

- the Spalding relationship in the intermediate buffer layer

$$y^+ = u^+ + e^{kB}\left[e^{ku^+} - 1 - ku^+ - \frac{(ku^+)^2}{2} - \frac{(ku^+)^3}{6}\right] \tag{5}$$

The boundary layer velocity profiles on the suction side (Figs. 14 and 15) evolve from laminar-like distributions (stations 6 and 8, $s/s_{max} = 0.14$ and 0.20), through intermediate stages characteristic of the transitional state (stations 12, 13, 14, 16, $s/s_{max} = 0.35$, 0.40, 0.46, 0.57), to the fully turbulent distributions, which fit well the

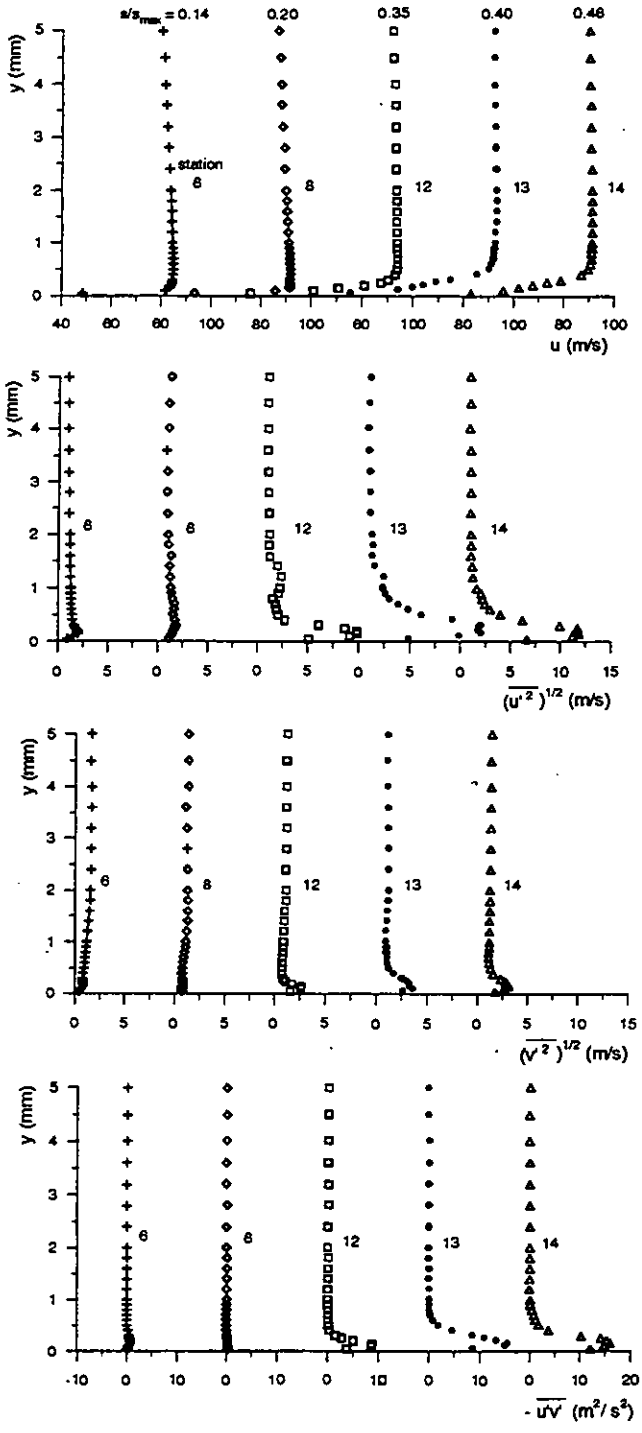

Fig. 12 Boundary layer profiles of mean velocity and Reynolds stress components: forward blade suction side

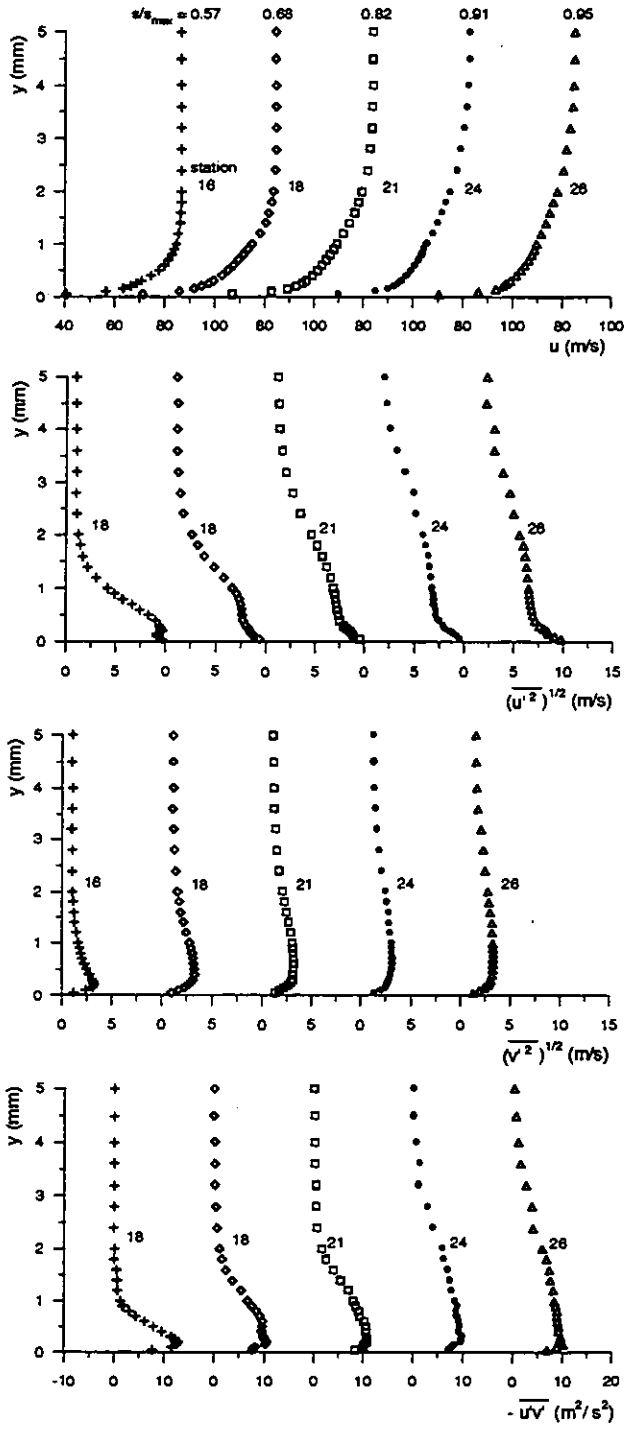

Fig. 13 Boundary layer profiles of mean velocity and Reynolds stress components: rear blade suction side

wall log law (stations 18, 21, 24, 26, $s/s_{max} = 0.68$, 0.82, 0.91, 0.95).

The evolutions of the streamwise and cross-stream turbulence intensities are also shown in Figs. 14 and 15.

The streamwise turbulence level in the laminar region is rather low, with a maximum of only 2.5 percent. At the onset of transition the peak value has grown to 11 percent, and in the transition region it has become larger than 13 percent, pointing out the occurrence of typical transitional amplified streamwise oscillations. The streamwise

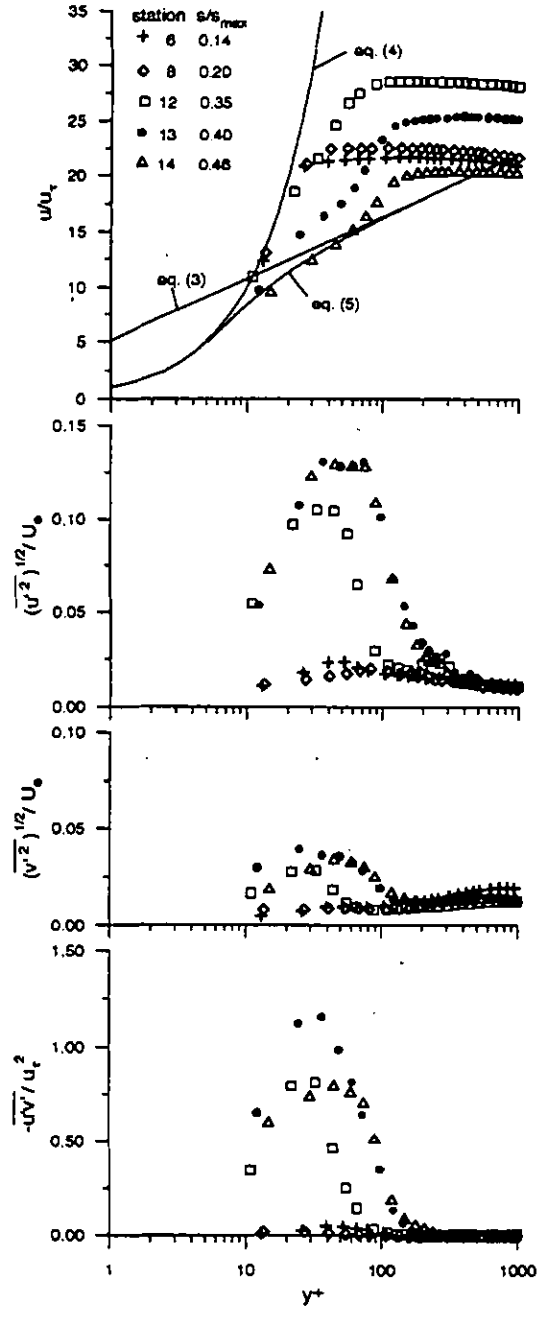

Fig. 14 Boundary layer profiles of dimensionless mean velocity and Reynolds stress components: forward blade suction side

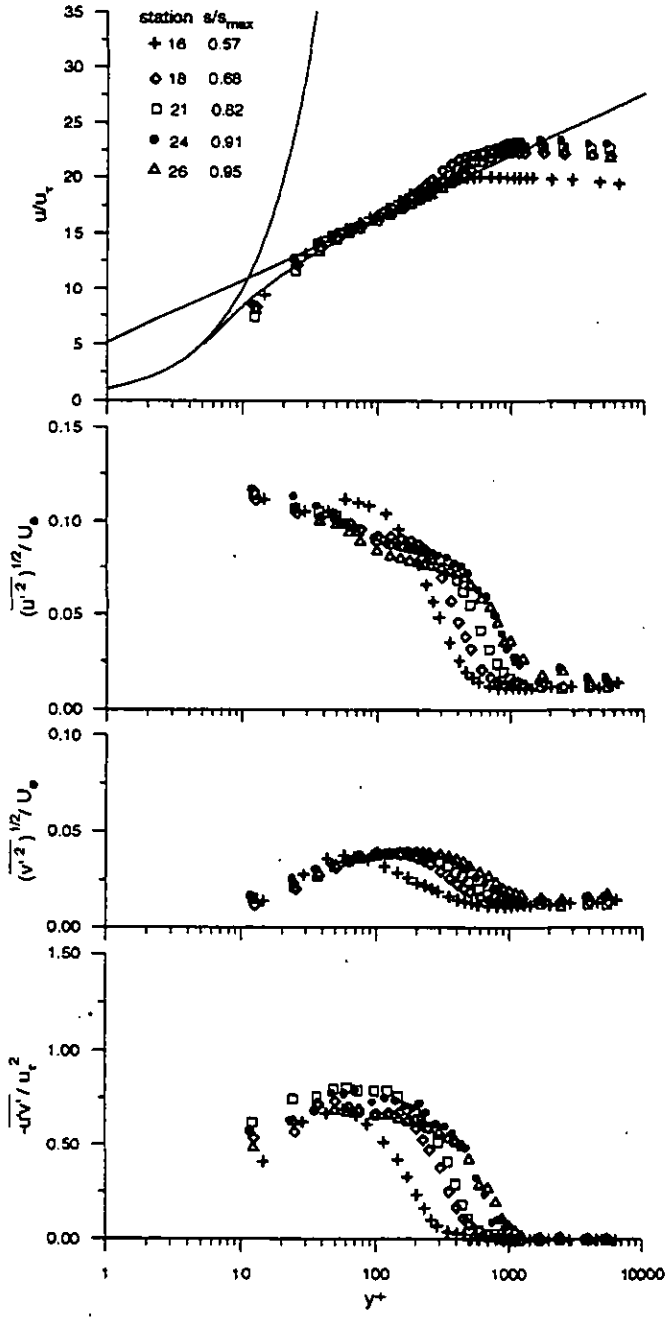

Fig. 15 Boundary layer profiles of dimensionless mean velocity and Reynolds stress components: rear blade suction side

turbulence shows a peak in the region $30 < y^+ < 60$, approximately in correspondence of the inflection of the mean velocity profile, while below $y^+ = 20$ the oscillations are damped by viscous effects. After the transition point the already observed typical double peak formation appears in the distribution (station 16, $s / s_{max} = 0.57$). At the end of transition the streamwise turbulence distributions change to a fully turbulent shape, similar to the flat plate turbulent boundary layer distribution (Klebanoff, 1955).

In the laminar region (stations 6 and 8), the cross-stream turbulence intensity remains at low levels, increasing continuously from the inner regions to the free-stream, in agreement with results of previous investigations (Zhou and Wang, 1993).

In the transitional region the cross-stream turbulence distributions show a peak at about the same position of the already observed streamwise turbulence peak, but the turbulence intensity remains always below 5 percent. In the turbulent region, the distributions are similar to that given by Klebanoff (1955): the shape is that of a

smooth hill with a maximum near $y^+ = 200$, corresponding to a hump of the streamwise turbulence profile, but the maximum level is nearly 10 percent lower than that of the reference case of Klebanoff. Maximum values of cross-stream turbulence intensity below 4 percent have been also found by Keller and Wang (1994) in flat plate boundary layers under accelerating flow conditions.

The comparison of the distributions for the two turbulence components points out that, due to the above observed peak of the streamwise fluctuating velocity, the turbulence anisotropy in the transition region is much larger than in the turbulent one.

In the transitional region the Reynolds shear stresses (Figs. 14 and 15) exhibit a significant increase in the range $10 \le y^+ \le 100$. At station 13 ($s/s_{max} = 0.40$) located between the onset of transition and the transition point (ST at $s/s_{max} = 0.35$; TP at $s/s_{max} = 0.48$), the maximum of Reynolds shear stress is about 20 percent larger than the wall shear stress. At station 14 ($s/s_{max} = 0.46$) very close to the transition point, the reduction of the peak value to about 80 percent is not due to the decrease of the Reynolds shear stress, but rather to the increase of the wall shear stress through the transition process (Fig. 11).

In the turbulent region the non-dimensional Reynolds shear stress distributions are similar to those given by Klebanoff (1955), but the levels in the present case are nearly 20 percent lower. This fact can be explained by considering that the the estimated values for the wall shear stress are larger than those corresponding to a zero pressure gradient equilibrium boundary layer. Results from the investigations of Keller and Wang (1994) in accelerating flow show that this tendency is enhanced by the increase of the acceleration parameter K.

Pressure Side Boundary Layer. An initial overview of the pressure side mean velocity and turbulence profiles in dimensional coordinates (Fig. 16) indicates that the boundary layer is exceedingly thin on this side and remains in laminar-transitional state from leading to trailing edge. However, the level of the streamwise fluctuating velocity appears to be very high, if compared with that observed in the laminar boundary layer on suction side.

The non-dimensional plots of Fig. 17 confirm that the mean velocity profiles are laminar-like until the blade trailing edge. This type of development induced by the accelerating flow has been observed in boundary layer investigations on the pressure side of turbine (e. g. Hodson , 1985 and Mee et al., 1990) and compressor cascades (Dong and Cumpsty, 1990).

The streamwise turbulence profiles show the most interesting features. The shape is typical of the laminar-transitional region with a maximum between $y^+ = 20$ and $y^+ = 40$, but the level is much larger (at least four times) than that of a laminar boundary layer: the peak value in fact ranges between 7 and 12 percent. A higher turbulence level could have be expected because of the concave curvature effect and the free-stream velocity lower than on the suction side. The results show that this high turbulence level does not apparently affect the shape of the laminar-like mean velocity profiles and the laminar boundary layer can support large turbulent fluctuations before undergoing transition.

A further confirmation about the nature of the pressure side boundary layer is given by the distributions of the cross-stream

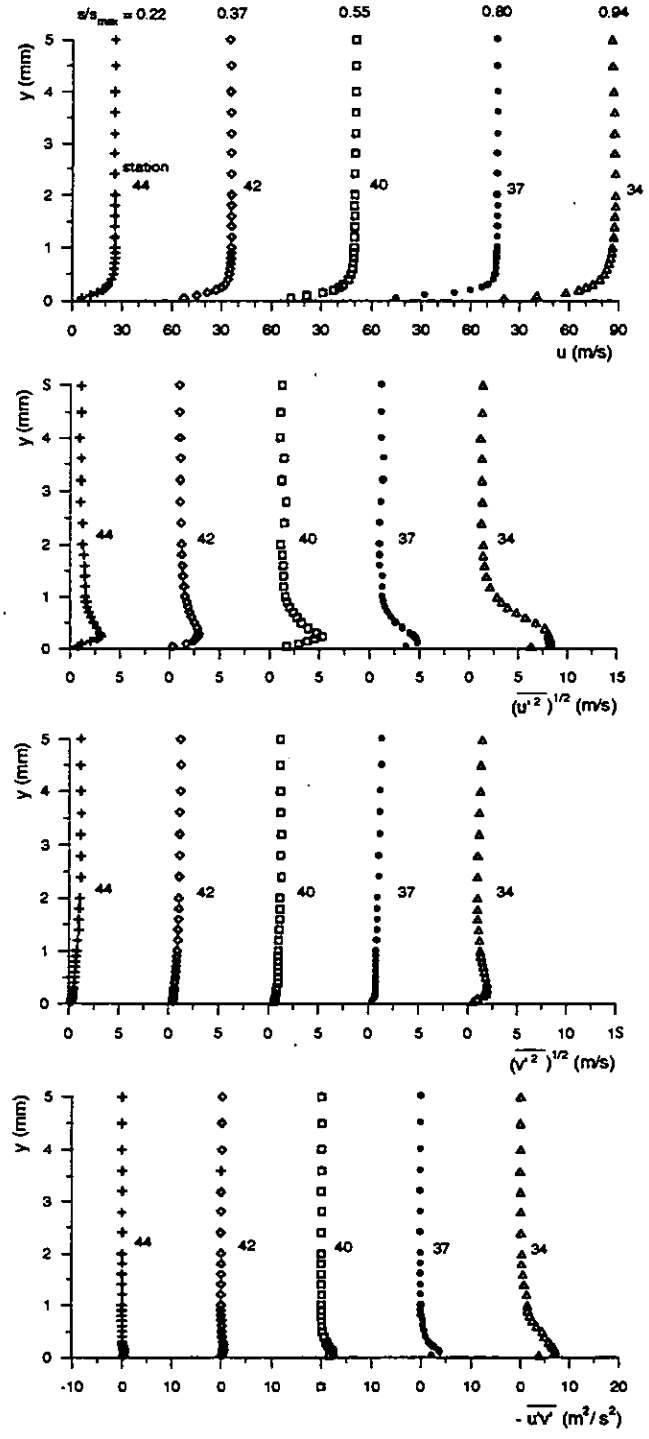

Fig. 16 Boundary layer profiles of mean velocity and Reynolds stress components: blade pressure side

turbulence intensity: both shape and level are those of a laminar boundary layer, as it can be deduced for instance by a comparison with the distributions for the laminar boundary layer on the forward suction side. The cross-stream turbulence intensity is about 1 percent near the wall and increases weakly towards the free-stream region.

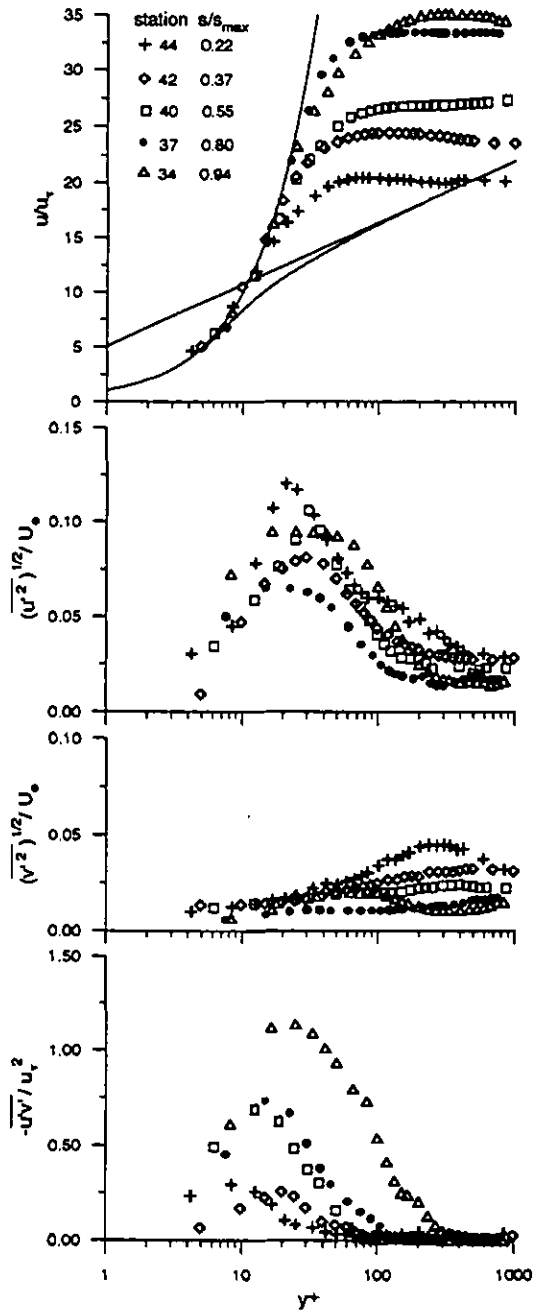

Fig. 17 Boundary layer profiles of dimensionless mean velocity and Reynolds stress components: blade pressure side

The Reynolds shear stress remains always below 75 percent of the wall shear stress, except at station 34 ($s/s_{max} = 0.94$), where it becomes larger than u_τ^2, in agreement with what has been observed for the suction side boundary layer at the transition onset.

4. CONCLUSIONS

Results of an experimental investigation of the profile boundary layer in a large scale turbine cascade have been presented. Measurements have been performed by means of a two-component fibre-optic laser Doppler velocimeter. Direct information on the boundary layer nature has been achieved by means of surface-mounted hot-film sensors.

Thanks to the large scale of the cascade and the non-intrusive nature of LDV, a large amount of velocity data have been obtained in the near wall region. Data were used to construct profiles of mean velocity and Reynolds stress components, describing in detail the boundary layer development on both suction and pressure sides.

Due to the high Reynolds number and the moderate flow deceleration, the suction side boundary layer becomes turbulent through a gradual transition process. In the transitional region mean velocity profiles develop continuously from laminar-like to turbulent-like.

During transition streamwise velocity oscillations result in an increase of streamwise turbulence intensity with peaks larger than 10 percent. Comparison between streamwise and cross-stream turbulence distributions shows that in the transitional region the flow becomes more anisotropic than in fully turbulent boundary layers.

In the early stage of transition a Reynolds shear stress peak separated from the wall exceeds the wall shear stress of about 20 percent. From this position the dimensionless Reynolds shear stress peak decreases, and the distribution changes to a typical turbulent boundary layer shape.

On the pressure side, the continuously accelerating flow makes laminar boundary layer velocity profiles compatible with large turbulence intensities. The boundary layer remains in fact in a laminar state until 80 percent of the pressure side surface lenght; from this position a transition process starts, which at the trailing edge is not yet completed. The level of the streamwise turbulence is very high compared with that observed in the laminar boundary layer on the suction side, but it is still lower than that found in the transitional reginn for the same side.

After the transition onset the streamwise turbulence peak is about 10 percent and the Reynolds shear stress exceeds the wall shear stress of 15 percent, showing that similar transition mechanisms occur on both sides.

The present results have been produced by the effort of documenting the viscous flow development within a large scale turbine cascade, whose trailing edge unsteady characteristics are being investigated in the framework of an European research program and whose geometry has been recently proposed as test case for time varying wake flow studies (Sieverding, 1994). These data can, therefore, be used as a comprehensive set of boundary conditions for detailed wake flow simulations or as an experimental contribution to the assessment of turbulence models to be employed in Navier Stokes calculations of turbine cascade flows.

ACKNOWLEDGEMENTS

This work is part of a research activity sponsored by the BRITE-EURAM Contract AER2-92-0048, endorsed by MTU Munich and SNECMA Paris. These supports are gratefully acknowledged.

The authors wish to thank Prof. Claus Sieverding of VKI and Dr. Thomas Schröder of MTU for advice and many useful discussions.

REFERENCES

Bellhouse, B. J., and Schultz, D. L., 1966, "Determination of mean and dynamic skin friction, separation and transition in low-speed flow with a thin-film heated element", *J. Fluid Mech.*, Vol. 24, part 2, pp. 379-400.

Boutier, A., 1991, "Accuracy of Laser Velocimetry", Lecture Series 1991-05, VKI, Brussels.

Buchhave, P., George, W., and Lumley, J., 1979, "The Measurement of Turbulence with the Laser Doppler Anemometer", Ann. Rev. Fluid Mech., n. 11.

Cicatelli, G., Sieverding, C. H., and Fevrier, N., 1994, "Test Case No 1 - Turbine Blade for Time Varying Wake Flow Studies", Lecture Series 1994-06, VKI, Brussels.

Cicatelli, G., and Sieverding, C. H., 1995," A Review of the Research on Unsteady Turbine Blade Wake Characteristics", AGARD PEP *85th Symposium on Loss Mechanisms and Unsteady Flows in Turbomachines*, Derby.

Deutsch, S., and Zierke, W. C., 1988, "The Measurement of Boundary Layers on a Compressor Blade in Cascade: Part 2 - Suction Surface Boundary Layers; Part 3 - Pressure Surface Boundary Layers and the Near Wake ", ASME *Journal of Turbomachinery*, Vol. 110, pp. 138-152.

Dong, Y., Cumpsty, N. A., 1990, "Compressor Blade Boundary Layers: Part 1 - Test Facility and Measurements With No Incident Wakes", ASME *Journal of Turbomachinery*, Vol. 112, pp. 222-230.

Elazar, Y., and Shreeve, R. P., 1990, "Viscous Flow in a Controlled Diffusion Compressor Cascade With Increasing Incidence", ASME *Journal of Turbomachinery*, Vol. 112, pp. 256-266.

Halstead, D. E., et al., 1995, "Boundary Layer Development in Axial Compressors and Turbines-Part 1 of 4: Composite Picture", ASME Paper No. 95-GT-461.

Hodson, H. P., 1983, "The Development of Unsteady Boundary Layers on the Rotor of an Axial-Flow Turbine", AGARD CP-351.

Hodson, H. P., 1985, "Boundary-Layer Transition and Separation Near the Leading Edge of a High-Speed Turbine Blade", ASME *Journal of Engineering for Gas Turbines and Power*, Vol. 107, pp. 127-134.

Hoheisel, H., Kiok R., Lichtfuss, H. J., and Fottner, L., 1987, "Influence of Free-Stream Turbulence and Blade Pressure Gradient on Boundary Layer and Loss Behavior of Turbine Cascades", ASME *Journal of Turbomachinery*, Vol. 109, pp. 210-219.

Hourmouziadis, J., Buckl, F., and Bergmann, P., 1987, "The Development of the Profile Boundary Layer in a Turbine Environment", ASME *Journal of Turbomachinery*, Vol. 109, pp. 286-295.

Hourmouziadis, J., 1989, "Aerodynamic Design of Low Pressure Turbines", AGARD Lecture Series, No. 167.

Karpuk, M., and Tiederman, W., 1976, "Effect of Finite-Size Probe Volume upon Laser Doppler Anemometer Measurements", *AIAA Journal*, Vol. 14, n. 8.

Keller, F. J., and Wang, T., 1994, "Flow and Heat Transfer Behavior in Transitional Boundary Layers with Streamwise Acceleration", ASME 94-GT-24.

Kim, J., Simon, T. W., Kestoras M., 1994,"Fluid Mechanics and Heat Transfer Measurements in Transitional Boundary Layers Conditionally Sampled on Intermittency", ASME *Journal of Turbomachinery*, Vol. 116, pp. 405-416.

Klebanoff, P. S., 1955,"Characteristics of Turbulence in a Boundary Layer with Zero Pressure Gradient", NACA Report 1247.

Mayle R. E., 1991, "The Role of Laminar-Turbulent Transition in Gas Turbine Engines", ASME *Journal of Turbomachinery*, Vol. 113, pp. 509-531.

Mee, D. J., Baines, N. C., and Oldfield, M.L.G., 1990, "Detailed Boundary Layer Measurements on a Transonic Turbine Cascade", ASME Paper No. 90-GT-263.

Modarress, D., Tan, H., and Nakayama, A., 1988, "Evaluation of Signal Processing Techniques in Laser Anemometry", *Fourth International Symposium on Application of Laser Anemometry to Fluid Dynamics*, Lisbon.

Oldfield, M. L. G., Kiock, R., Holmes, A. T., and Graham C. G., 1981, "Boundary Layer Studies on Highly Loaded Cascades using Heated Thin Films and a Traversing Probe", ASME *Journal of Engineering for Power*, Vol. 103, pp. 237-246.

Pucher P., and Göhl, R., 1987, "Experimental Investigation of Boundary Layer Separation With Heated Thin-Film Sensors", ASME *Journal of Turbomachinery*, Vol. 109, pp. 303-309.

Schröder, Th., 1991, "Investigations of Blade Row Interaction and Boundary Layer Transition Phenomena in a Multistage Aero Engine Low-Pressure Turbine by Measurements with Hot-Film Probes and Surface-Mounted Hot-Film Gauges", Lecture Series 1991-06, VKI, Brussels.

Schulz, H. D., Gallus, H. E., and Lakshminarayana, B., 1990, "Three-Dimensional Separated Flow Field in the Endwall Region of an Annular Compressor Cascade in the Presence of Rotor-Stator Interaction: Part 1- Quasi-Steady Flow Field and Comparison with Steady-State Data", ASME *Journal of Turbomachinery*, Vol. 112, pp. 669-678.

Sharma, O. P., Wells, R. A., Schlinker, R. H., and Bailey D. A., 1982, "Boundary Layer Development on Turbine Airfoil Suction Surfaces", ASME *Journal of Engineering for Power*, Vol. 104, pp. 698-706.

Sieverding, C. H., and Heinemann, H., 1989, "The Influence of Boundary Layer State on Vortex Shedding from Flat Plates and Turbine Cascades", ASME Paper No. 89-GT-296.

Sieverding, C. H., 1994,"Numerical Methods for Flow Calculation in Turbomachines", Lecture Series 1994-06,VKI, Brussels.

Strazisar, T., 1986, "Laser Anemometry in Compressors and Turbines", ASME Lecture on Fluid Dynamics of Turbomachinery.

Thwaites, B, 1949, "Approximate Calculation of the Laminar Boundary Layer", *Aeronautical Quarterly*, Vol. 1, pp. 245-280.

White, F. M., 1991, *Viscous Fluid Flow*, McGraw-Hill, Singapore.

Wunderwald, D., and Fottner, L., 1995, "Experimental Investigation of Boundary Layer Transition and Turbulence Structures on a Highly Loaded Compressor Cascade", ASME Paper 95-GT-129.

Zhou, D., and Wang, T., 1993, "Effects of Elevated Free-Stream Turbulence on Flow and Thermal Turbulence on Flow and Thermal Structures in Transitional Boundary Layers", ASME Paper No. 93-GT-66.